2022 9th IEEE RAS/EMBS International Conference for Biomedical Robotics and Biomechatronics (BioRob) | 978-1-6654-5849-8/22/$31.00 ©2022 IEEE | DOI: 10.1109/BIOROB52689.2022.9925384

A 3-D Haptic Trackball Interface for Teleoperating Continuum Robots

Mufeng Xie[1], Cédric Girerd[1], Tania K. Morimoto[2]

***Abstract*—Continuum robots offer many advantages for navigation in constrained environments, due to their flexible backbone and ability to conform to complex shapes. However, their non-intuitive kinematics can lead to challenges in the design and mapping strategies used for human-in-the-loop control interfaces. In this paper, we propose a new 3-D haptic trackball interface that is specifically designed to be both an input and feedback device for teleoperating continuum robots. The system allows the operator to control the tip position of the robot with high accuracy over a large workspace, and it provides haptic feedback, when necessary, in order to assist the operator with performing various tasks. A subjective study was conducted to evaluate the performance of the proposed interface compared to a commercially available system and to evaluate the effects of providing haptic feedback. The interfaces were used to perform two different teleoperation tasks, and the new haptic trackball interface resulted in higher accuracy and improved obstacle avoidance, illustrating its potential as a more effective teleoperation interface.**

***Index Terms*—Surgical Robotics: Steerable Catheters/Needles, Haptics and Haptic Interfaces.**

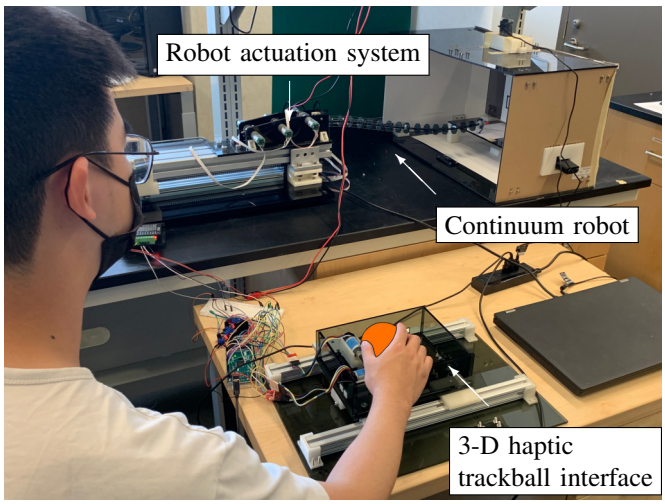

Fig. 1. An operator uses the proposed haptic trackball interface to control a tendon-driven continuum robot.

I. Introduction

CONTINUUM robots are characterized by their continuously bending backbone, often inspired from biological structures, such as trunks or tentacles [1], [2]. Unlike conventional manipulators, continuum robots are not composed of discrete rigid links and joints. This continuum structure allows them to conform to complex shapes and to navigate through constrained and highly curved environments [3], [4], motivating their use in many medical applications. A human-in-the-loop teleoperation scheme is typically used to control these continuum robots [2]. Compared to traditional rigid-linked robots, controlling continuum robots can become non-intuitive due to their complex kinematics, which are highly dissimilar compared to those of the human operator. However, to date there has been only limited research investigating and evaluating input devices for teleoperating continuum robots [2], [5].

Thus far, commercially available input devices are typically used. For instance, joysticks, which are portable and simple [6], are commonly used to control the robot tip. However, the limited joystick workspace usually results in the use of a position to velocity (P2V) mapping, where the position of the input device is mapped to the velocity of the robot [7], [8]. Compared to interfaces that use a position to position (P2P) mapping, where the position of the input device is mapped to the position of the robot, P2V mappings typically result in less accurate position control [8]. Another approach has been to use commercially available input devices featuring a pen-like stylus, such as the Geomagic Touch (formerly Phantom Omni) [5], [9], [10]. Typically, a P2P mapping is used, resulting in high position control accuracy, however, there are kinematic and workspace mismatches between these devices and the robots to be controlled. The development of input devices specifically designed for control of continuum robots could help overcome challenges with using those that are commercially available.

Recent work has begun to investigate alternative input device designs. One approach has been to design a custom device with a kinematic structure similar to that of the continuum robot to be controlled [11], [12], [13]. These devices consist of continuum segments that when bent or shaped by the user are mapped to changes in the robot position, shape, or speed. The interface in [12], for example, is a single, flexible, 3-D printed structure that can bend similarly to the distal end of the growing robot it is designed to control. The interface in [13] consists of three sections designed to emulate a three-segment continuum robot. These devices are designed with the goal of creating a more intuitive interaction for users in order to improve overall performance.

In addition to the design architecture and mapping strategy, haptic feedback also has the potential to help improve task performance, particularly with regards to safety and accuracy [14]. For continuum robots, studies have shown that

[1]Mufeng Xie and Cédric Girerd are with the Department of Mechanical and Aerospace Engineering, University of California, San Diego, La Jolla, CA 92093 USA. xmufeng@ucsd.eng.edu

[2]Tania. K. Morimoto is with the Department of Mechanical and Aerospace Engineering and the Department of Surgery, University of California, San Diego, La Jolla, CA 92093 USA. tkmorimoto@eng.ucsd.edu

although people are capable of operating them using visual feedback alone, many feel that haptic feedback would be advantageous [15]. Despite this potential, there has been little work to date that investigates the addition of haptic feedback for continuum robot teleoperation. Even studies that use commercial input devices capable of providing haptic feedback (e.g. the Geomagic Touch), tend to use them solely as an input device, while just a limited number take advantage of the haptic feedback capabilities [16].

In this paper, we propose a 3-D haptic trackball interface (Fig. 1) that can be used to control the position of the robot tip and to provide haptic feedback, both in 3 DOF. The key features of the proposed design are (1) the architecture of the interface, along with the mapping strategy, enable accurate position control across a large workspace; and (2) the ability to provide kinesthetic haptic feedback to the operator can help improve task performance and safety. We evaluate the proposed interface by conducting a user study and comparing the performance during path-following and obstacle-avoidance tasks against the performance using a conventional joystick. The results of the study illustrate that our interface can enable improved precision and obstacle avoidance during these tasks.

The rest of this paper is organized as follows. Section II presents the design of our proposed interface, and Section III explains the mapping schemes between the interface and the robot we control. We explain the experimental study in Section IV and results are discussed in Section V. Finally, Section VI presents the current limitations and future works.

II. System Design

Our proposed interface can be divided into two parts: a 2 DOF trackball and a 1 DOF translation mechanism. The two components are bidirectional, designed as both input and feedback mechanisms. The trackball component controls and provides feedback for the in-plane motions of the robot tip, where moving the trackball forward and backward moves the robot tip up and down (Fig. 2(a)) and moving the trackball left and right moves the robot tip left and right (Fig. 2(b)). The translation mechanism controls and provides feedback for the insertion and retraction of the robot (Fig. 2(c)).

A. Trackball Design

Previous work has investigated device architectures similar to the trackball portion of our interface, which contains a sphere driven by rolling disks [17]. In particular these devices have been designed to enable applications requiring large workspaces [8], [18] and as more general haptic devices [19], [20], [21]. Our design, shown in Fig. 3, uses a similar friction-drive mechanism for the 2-D trackball portion of the device. We use two 12 V HP motors with 48 CPR encoders from Pololu for the actuators. These motors are backdrivable so that the user can rotate the trackball to provide input in any direction. 3-D printed shafts are press-fit onto the motor shafts, and two additional, passive (non-driven) shafts are attached opposite to these (see Fig. 3). All shafts are 8 mm in diameter and are wrapped with neoprene tubing to increase the friction between the shaft and the trackball, which is critical for ensuring the transmission of forces between the two. Users are also trained to apply a light downward force to ensure that the trackball maintains contact and does not come out of the housing. The trackball is located on top of the four shafts and is 76.2 mm in diameter and made from polyurethane. Encoders are attached to the two motors and are used to measure the change in motor position due to both user input, as well as due to commanded motor movements needed to provide feedback.

B. Translation Mechanism Design

The components comprising the trackball mechanism are housed in a 150 mm $\times$ 200 mm carriage, as shown in Fig. 3. The translation of this entire carriage is achieved via a capstan-drive mechanism located underneath. A 8 mm diameter capstan is connected to another 12 V HP motor with 48 CPR encoder, and a 0.23 mm diameter, plastic-coated steel cable is wound around the capstan once, with the two ends of the cable then fixed to either end of the carriage. Capstan drive is used due to the absence of backlash, low inertia, and high stiffness in the motion transmission. An aluminum track is used to guide the translation of the carriage, and the total travel length is designed to be 150 mm. When the user moves the carriage along the aluminum track, the position is

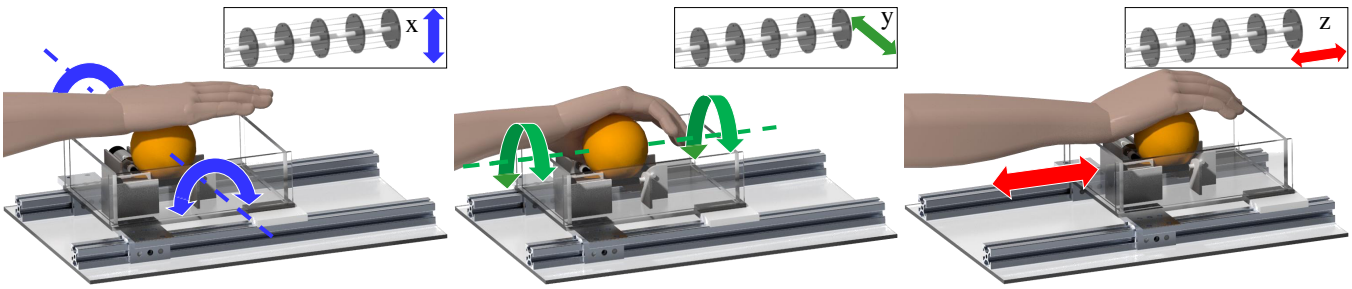

(a) (b) (c)

Fig. 2. Illustration of the haptic interface developed and the mapping between the user motions and the displacements of the tip of the continuum robot. (a) Moving the trackball forward and backward maps to movement of the robot tip up and down (along the x-axis). (b) Moving the trackball left and right maps to movement of the robot tip left and right (along the y-axis). (c) Moving the entire trackball via the translation mechanism maps to inserting and retracting the robot (along the z-axis).

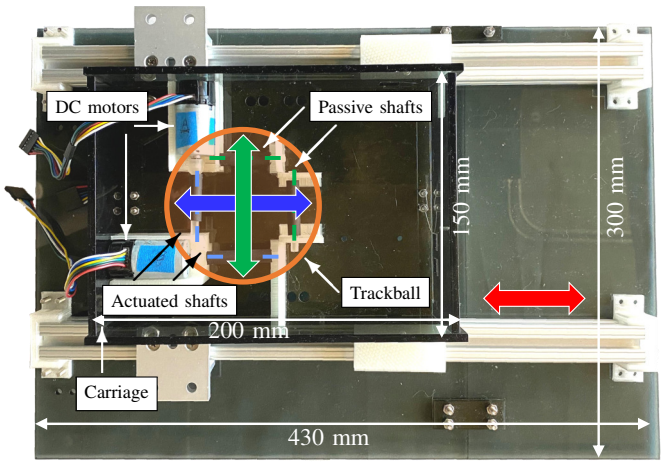

Fig. 3. An overview of the 3-D haptic trackball interface with critical dimensions. The trackball interacts with two DC motors via friction drive, and this entire mechanism is housed in a carriage that can move linearly along a set of rails via capstan drive. The blue, green, and red arrows correspond to motion of the robot tip along the x, y, and z directions, respectively.

again measured using the encoder from the associated motor. Similarly, force feedback can be applied by controlling the motor to drive the trackball carriage in the desired direction.

III. Teleoperation Scheme

We then use our 3-D haptic trackball to teleoperate a tendon-driven continuum robot. Compared to simulations, the robot provides a realistic physical platform, consistent with the end-use of our interface. To do so, we create a mapping from user input to robot tip movement, as well as an approach to provide force feedback to the user based on environment interactions.

A. Robot Kinematics

The tendon-driven robot used in this work is 30 mm in diameter and consists of two sections, as shown in Fig. 4(a). Each section consists of a set of disks equally spaced (30 mm apart) along a flexible backbone. The lengths of the sections are 250 mm and 240 mm, for the proximal and distal sections, respectively. Two sets of 3 tendons are routed along the length of the robot from the base at a distance of 13 mm from the backbone. One set is attached to the most distal disk in the proximal section and the other set to the most distal disk in the distal section. The tendons in each set are arranged radially, each 120° apart. By changing the lengths of the tendons, the shape of the robot, and thus the tip position, can be controlled.

In addition, the entire robot can be translated along a single axis. The addition of this degree of freedom is important in many medical applications, where the robot may need to navigate from an entry point to a target region deeper within the body. To achieve translation, a carriage is designed to house the entire tendon-driven robot described above, including the motors used to actuate the tendons. This carriage is then attached to a linear actuator driven by a Nema23 stepper motor and controlled using an Arduino Mega.

The parameters of continuum robots are defined in three spaces: actuator space, configuration space, and task space. We propose to teleoperate the robot in task space, where user inputs to the 3-D trackball interface map directly to the robot tip position. Given the desired change in robot tip position, we must use the inverse kinematics to determine the corresponding actuator space parameters, $\mathbf{q}^\intercal = \begin{bmatrix}\mathbf{q}_l & \mathbf{q}_s\end{bmatrix}$. Since the dimension of the actuator space is 7 and the dimension of the task space in which the robot is controlled is 3, solutions to the inverse kinematics problem are not unique, and a root finding method on the direct kinematics model is typically used.

We start by expressing the direct kinematics model of the tendon-driven portion of the robot. For a constant-curvature section i, the arc parameters r_i, ϕ_i, θ_i can be obtained from the cable lengths, $\mathbf{q}_l$, using geometric relations detailed in [22]. The homogeneous transformation matrix corresponding to this single constant-curvature section is given by Eq. (1) [22]

$$\mathbf{T}_i = \begin{bmatrix}\mathbf{R}_z(\phi_i) & 0\\ 0 & 1\end{bmatrix}\begin{bmatrix}\mathbf{R}_y(\theta_i) & \mathbf{p}_i\\ 0 & 1\end{bmatrix}, \tag{1}$$

where

$$\mathbf{p}_i^\intercal = \begin{bmatrix}r_i(1-\cos\theta_i) & 0 & r_i\sin\theta_i\end{bmatrix} \tag{2}$$

and $\mathbf{R}_y(\theta_i), \mathbf{R}_z(\phi_i)$ are 3-D rotation matrices of angles θ_i and ϕ_i about the axes y and z, respectively, with the angles ϕ_i and θ_i defined in Fig. 4(a). The forward kinematics of our two segment tendon-driven robot is then given by $\mathbf{T} = \mathbf{T}_1\mathbf{T}_2$. In

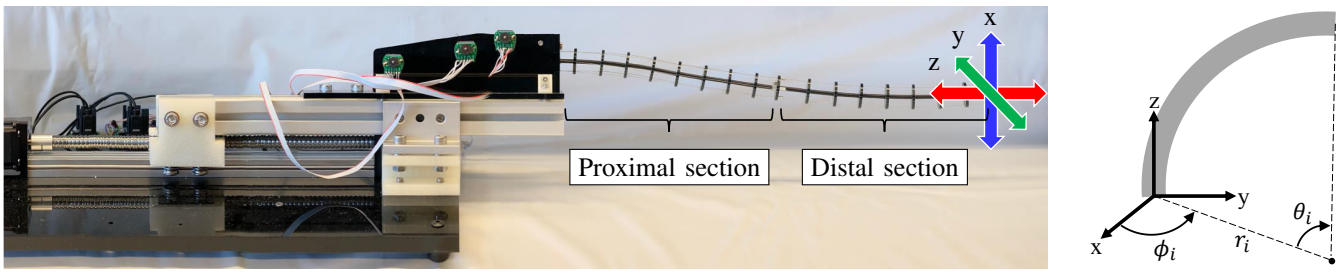

(a) (b)

Fig. 4. (a) Side view of the two-segment, tendon-driven continuum robot. (b) Representation of a single segment of the robot, including the relevant arc parameters.

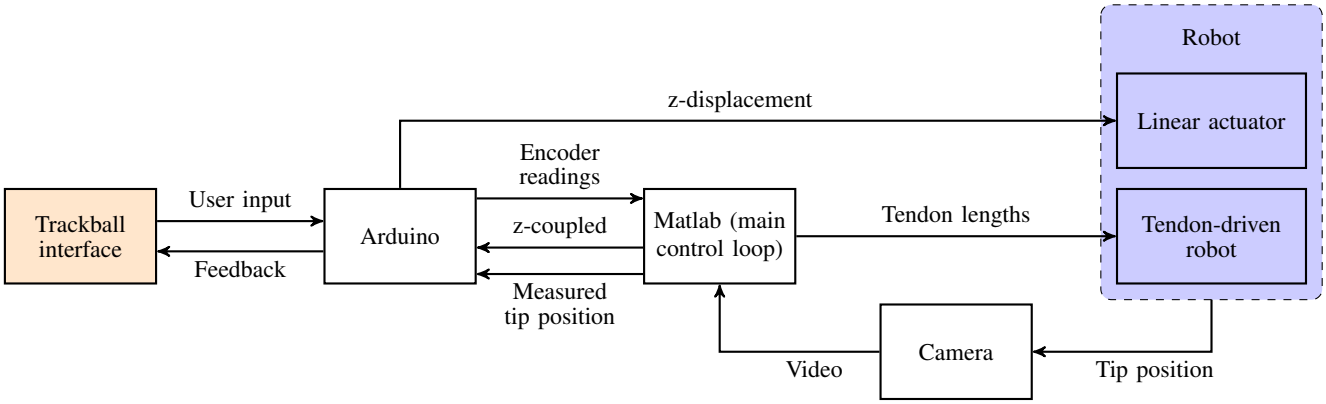

Fig. 5. Diagram of the system workflow. As users interact with the trackball interface, the changes in the tendon lengths and z-axis position required to achieve the desired robot tip position are computed. A vision-based system is used to determine the actual robot tip position, and this measurement is then used to determine the magnitude and direction of force feedback to render to the user.

this work, we used a simplified version of the kinematics in [22], where the curvatures of both robot segments are equal.

Using the above formulation, we can then solve for the inverse kinematics of the entire robot to obtain the necessary actuator space parameters. To do so, we first solve for the arc parameters using the Newton-Raphson algorithm based on the tip coordinates of the tendon-driven robot in the $x-y$ plane. We then determine the cable lengths $\mathbf{q}_l$ using geometric relationships detailed in [22]. Finally, we inject the obtained arc parameters in the z-coordinate of the tendon-driven robot, and define the slider position as the difference between the z coordinate of the desired tip position and this calculated value.

B. Haptic Feedback

Our interface can provide force feedback in 3 DOF — 2 DOF using the trackball and 1 DOF using the translation mechanism. In both cases, we must first compute the desired force to be rendered to the user, and based on this force, we can then compute the required motor torque. In this work, we compute the desired force as a force that is normal to the surface being penetrated and that has a magnitude determined using a simple spring model, as given in Eq. (3)

$$F = k \cdot \Delta d, \tag{3}$$

where k is defined to be 500 N/m. This stiffness was selected to ensure that the force feedback is noticeable without causing the system to go unstable. The amount of penetration, Δd, is computed based on the difference between the robot tip position and the surface being penetrated, as explained in detail in Section IV.

The motor torques required to render the desired forces in each direction can then be computed. As shown in Fig. 6, assuming quasi-static conditions and neglecting forces on the trackball due to interaction with the shafts orthogonal to the direction of motion, the force tangent to the surface of the trackball, $F_{trackball}$, is then equal to the force tangent to the

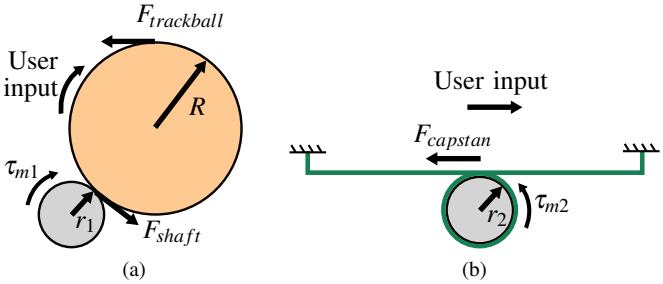

Fig. 6. Schematics illustrating the mechanism for generating force feedback for (a) a single degree of freedom for the trackball interface and for (b) the capstan system.

surface of the motor shaft, F_{shaft}, at the point of contact. The torque required to render a desired force in either the x- or y-directions is therefore calculated as $\tau_{m1} = F_{trackball} \cdot r_1$. Similarly for the z-direction, as the user pushes the carriage, a force, $F_{capstan}$, can be rendered in the opposite direction to motion via capstan drive. The motor torque required to achieve the desired force is calculated as $\tau_{m2} = F_{capstan} \cdot r_2$.

C. Control

The overall control scheme is shown in Fig. 5. User input from the trackball interface is determined based on encoder readings from the associated motors, which are read using an Arduino. These signals are sent via serial port communication to the main control loop, which runs in MATLAB. Based on the inverse kinematics, the necessary tendon lengths and linear slider position are calculated and commanded to the robot, causing its tip to move. We then measure the actual tip position using a set of two orthogonal cameras (Logitech C922 pro). The tracking method is a color-based algorithm that identifies a 5 mm radius red sphere that is attached to the robot tip (see Fig. 7 and Fig. 9) and that is visually distinct from the background. This tracking method is used, rather than relying on the tip position given by the kinematics model, due to model inaccuracies, including the assumption of constant curvature for the robot sections. Based on the

measured tip position, we calculate the magnitude and direction of the force feedback, and render the feedback to the user through the trackball interface.

IV. Experimental Study

We performed a user study to evaluate the performance of our proposed interface. We designed two tasks: (1) path following and (2) obstacle avoidance. Each task was performed using three user interfaces: the 3-D trackball interface with haptic feedback, the 3-D trackball interface without haptic feedback, and off-the-shelf joysticks.

A. Joystick Setup

The joysticks used for comparison are part of a Logitech F310 gamepad. To enable a fair comparison, a P2P mapping is implemented for the x-axis and y-axis, similar to the mapping for the trackball interface. However, because the maximum deployment along the z-axis is relatively long, and position mapping may not apply for such joystick mechanisms due to their limited workspace, we make the mapping on the z-axis a velocity mapping. This mapping, although not consistent on the joystick setup, remains intuitive for users based on pilot tests conducted prior to the official study. An additional design feature for the joystick setup includes a clutch button, which was implemented to allow the user to release the joystick without having the robot snap back to the center position if released. When the user pushes the joystick to any position and presses the clutch button, the joystick can be released without impacting the tip position. When the clutch button is later released, the tip of the robot is controlled from the current joystick position. The clutch button is set to be the right trigger on the gamepad and is considered to be a comfortable gesture for most right-handed users.

B. Tasks

1) Path-Following Task: For this task, participants are asked to control the robot to follow a given path that is split into two parts, located in two orthogonal planes. Planar paths are used to simplify the display of the desired path to the user. The first part of the path is in the $y-z$ plane (see Fig. 7). To avoid the effects of viewing angle, participants see the path from a real-time video provided by an overhead camera. Once participants reach the endpoint of the first part of the path, they then follow the second portion located in the $x-y$ plane. Since users are directly facing this portion, no external camera view is provided.

Participants are asked to use the 3 different user interfaces, for 3 trials each. For the case when force feedback is applied, we define a tolerance region with virtual walls located a distance of 5 mm on each side of the path, as represented in Fig. 8 for the case of a path on the $y-z$ plane. This tolerance was selected based on the tradeoffs of not being too strict on requiring users to follow the path perfectly, while still

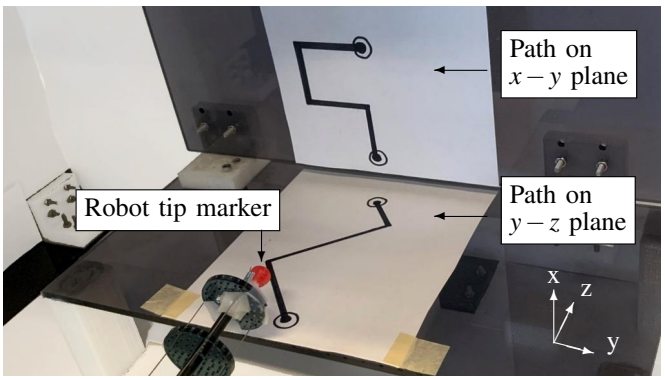

Fig. 7. Experimental setup for the path following task, with the first part of the path lying in the $y-z$ plane, and the second part of the path lying in the $x-y$ plane.

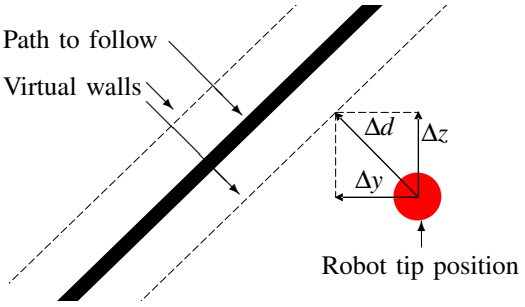

Fig. 8. Representation of the distances in the $y-z$ plane, used to render force feedback in the path-following task, when the robot tip is outside of the tolerance area.

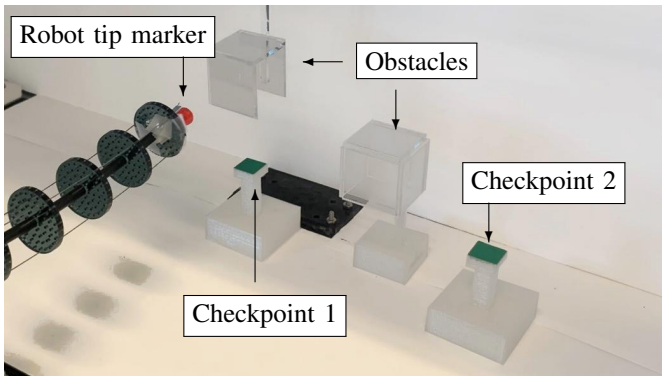

Fig. 9. Experimental setup for the obstacle-avoidance task. Participants must navigate to two sequential checkpoints, shown in green, while avoiding all obstacles, represented by acrylic cubes.

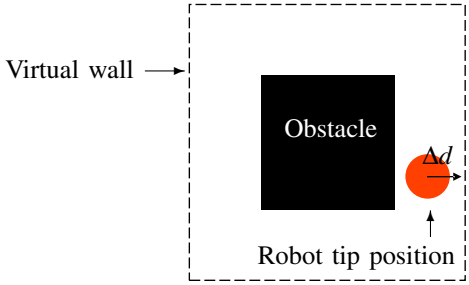

Fig. 10. Representation of the distances used to render force feedback in the obstacle-avoidance task, when the robot tip is too close to the obstacles.

ensuring that the force feedback would remain noticeable. If the robot tip is commanded to move away from the path beyond this tolerance region, force feedback is rendered in order to guide users back towards the path. For feedback in the $y-z$ plane, for example, Δd is the distance between the measured tip position and the virtual wall, decomposed into two normal directions $(\Delta y, \Delta z)$. Force feedback is thus $F_y = k\Delta y$ and $F_z = k\Delta z$, where $k = 500$ N/m.

2) Obstacle-Avoidance Task: In this task, participants are asked to control the robot to move from a starting point to sequential checkpoints, while avoiding the obstacles in between. The workspace setup is shown in Fig. 9, where the 30 mm $\times$ 30 mm $\times$ 30 mm clear boxes represent obstacles and the 10 mm $\times$ 10 mm green squares are checkpoints. Participants are again asked to use the 3 different user interfaces, for 3 trials each. Force feedback is again computed using Eq. (3), where $k = 500$ N/m and Δd is the distance between the measured tip position and virtual walls located at a distance of 5 mm from the obstacles, as shown in Fig. 10. The virtual walls are used to try to warn the users of the obstacles prior to any collisions.

C. Evaluation Metrics

For every trial of both tasks, we record a data vector $\mathbf{v} = [x_1, y_1, z_1, h_1, m_1, s_1, \ldots, x_N, y_N, z_N, h_N, m_N, s_N]$, where N is the total number of points on the actual trajectory. The coordinates of the n-th point on the trajectory are given by (x_n, y_n, z_n) and the time the n-th point is reached (hour, minute, and second, respectively) is given by (h_n, m_n, s_n).

For the path-following task, the primary evaluation metric is the error between the user's actual path and the desired path. The error for the j-th trial of the i-th user is calculated as in Eq. (4)

$$E_{ij} = \frac{1}{N}\sum_{n=1}^{N} dist(\mathbf{p_{tip,n}}, \texttt{Path}), \tag{4}$$

where $\mathbf{p_{tip,n}}$ is a point on the actual trajectory, `Path` is the given path to follow, and $dist(\mathbf{p_{tip,n}}, \texttt{Path})$ is the shortest distance from a point $\mathbf{p_{tip,n}}$ to the line in `Path`. The overall mean error of user i is then given by Eq. (5).

$$E_i = \frac{1}{3}\sum_{j=1}^{3} E_{ij} \tag{5}$$

Finally, for a given user interface, the mean error, $\bar{E}$, across M users is given by Eq. (6)

$$\bar{E} = \frac{1}{M}\sum_{i=1}^{M} E_i. \tag{6}$$

For the obstacle-avoidance task, the primary metric is the number of collisions. During each trial, the instructor of the study records in real-time each instance where an obstacle is hit. Each instance, and the total number, are subsequently verified offline by analyzing the actual trajectory data collected. Finally, for both the path-following and obstacle-avoidance tasks, the total time to complete the tasks is calculated based on the recorded time data.

V. Results and Discussion

Data was analyzed from $M = 12$ right-handed adults (23.6 ± 2.9 years old, 3 females and 9 males) who performed the study after giving informed consent, under a protocol approved by the University of California, San Diego Institutional Review Board (IRB protocol 190381). Each participant completed the two tasks using the three different user interfaces, three times each. To minimize order effects, a Latin Square is used for the user interfaces, and a balanced design is used for the two tasks.

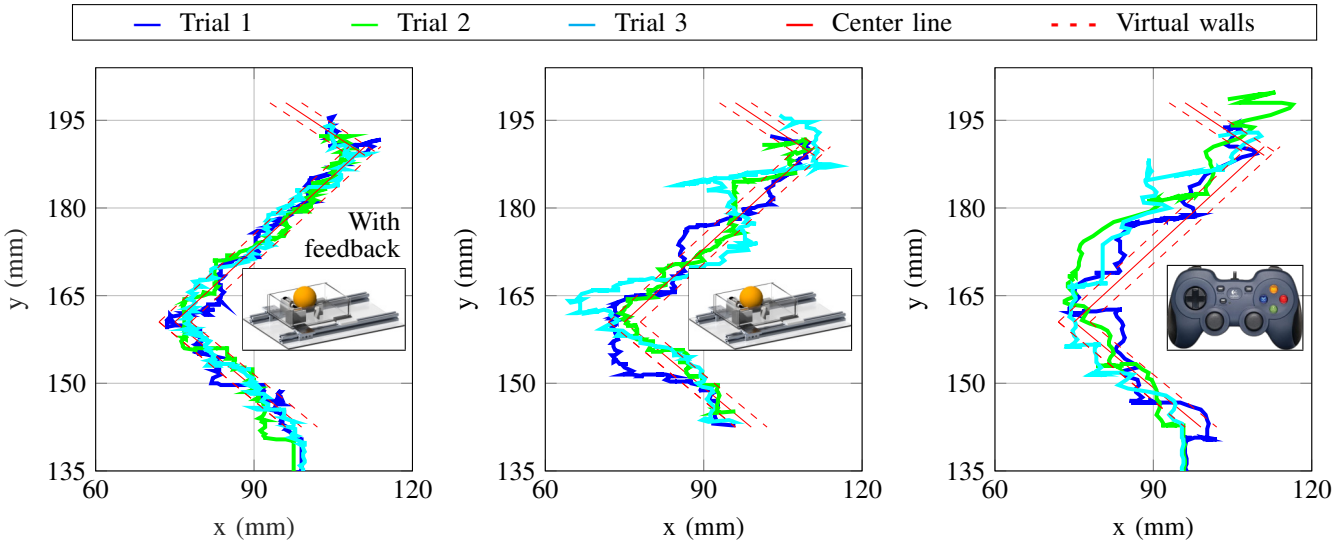

Fig. 11. Representative examples of the robot tip trajectory for a single user when following the first part of the path using (a) the proposed haptic interface with force feedback, (b) the proposed interface without force feedback, and (c) a joystick.

A. Path-following Task

Representative examples of robot tip trajectories during the first part of the path when using (a) the trackball interface with haptic feedback, (b) the trackball interface without haptic feedback, and (c) the joysticks are shown in Fig. 11. In each plot, the solid lines in blue, green, and cyan represent the actual trajectories for the 3 trials of a user. The solid red line represents the desired path, and the dashed red lines show the boundaries for force feedback. From the plots, we can qualitatively verify that the trackball with force feedback performs the best in terms of staying within the boundaries of the given path among all user interfaces tested. In addition, a boxplot of the errors can be seen in Fig. 12a, confirming the previous observations that the trackball interface with feedback results in the highest accuracy during path following.

To determine whether there is a statistically significant difference between the three user interfaces, we perform a Shapiro–Wilk test to check for normality of the data. Neither path error or completion time are found to be normally distributed, so we next conduct Kruskal-Wallis tests. The p-value for the path error data is found to be 0.0011, which indicates a 99% confidence level of significant difference among the three user interfaces. To determine which user interface is significantly different from the others, we then conduct a Mann-Whitney test with Bonferroni correction between each pair of user interfaces. The only statistically significant difference was between the trackball with feedback and the joystick, with a p-value of 0.0012. From the above analysis, we can conclude that compared to using an off-the-shelf joystick, the trackball interface with force feedback results in significantly less error.

For the time data, the p-value from the Kruskal-Wallis test is 0.013, which indicates a 95% confidence level of significant difference among the three user interfaces. A Mann-Whitney test with Bonferroni correction was performed, giving a p-value of 0.012 between the trackball with feedback and the joystick, indicating a statistically significant difference. A comparison of the completion times can also be seen in the boxplot in Fig. 12b. The longer task completion times observed when using the trackball with force feedback could be due to several possible factors. First, it is possible that when users feel the force feedback, they then spend extra time to correct the robot tip trajectory. It is also possible that users become more cautious by slowing down their movements once they experience the feedback. Finally, it should be noted that participants were not asked to try to complete the task quickly, and with additional training time, it is likely that overall task completion time would be decreased.

B. Obstacle-Avoidance Task

For the obstacle-avoidance task, we record the number of times that the robot tip hits obstacles in each trial. This data shows that 75% of users did not hit any obstacle during the three trials for the trackball with force feedback, compared to 58% for the trackball without force feedback, and 50% for the joystick. These results show that the trackball with force feedback enables improved obstacle avoidance. Finally, the time required for the users to complete the obstacle-avoidance task is represented in the boxplot visible in Fig. 12c. These runtime results tend to indicate that our haptic interface takes more time to operate compared to the other interfaces. We ran the Kruskal-Wallis test for the runtime but found no statistically significant difference among the three user interfaces ($p = 0.249$).

C. Post-Study Survey

At the end of the study, each participant was asked to complete a post-study survey, which consisted of a series of subjective questions asking for either yes/no responses or for a ranking of different devices from 1 to 5. We found that 9 out of the 12 users had experience with video games or input devices with at least 3 DOFs prior to participating in the user study, indicating that most participants had a basic understanding of hand-eye coordination. We asked users to rate and rank the three user interfaces based on various aspects, including precision, speed control, mental effort, smoothness and general comfort. The results show that, in general, participants felt that the trackball interface, both with and without force feedback, perform similarly, and that they

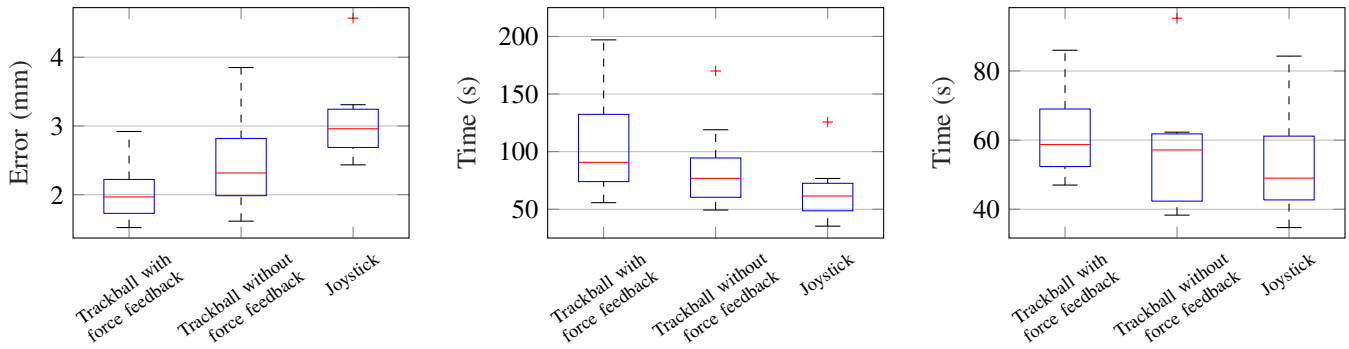

Fig. 12. (a) Boxplot representing the errors during the path following experiment, (b) the time required to complete the path following experiment, and (c) the time required to complete the obstacle avoidance experiment. These boxplots are for each user interface and for all participants.

are both better than the joystick. The only exception concerns the mental effort required to operate these two user interfaces. Users rated the trackball interface with force feedback as the most mental-effort-consuming interface, and the joystick as the least. This result is reasonable given that most users have prior experience with video games and are therefore familiar with using joysticks. Additional training time with the trackball interface could potentially help to decrease the mental load required in the future.

VI. Conclusion

We developed a novel 3-D haptic trackball interface for controlling continuum robots. The interface was successfully used to teleoperate the tip position of a tendon-driven robot and provide haptic feedback to assist with task performance. We evaluated the performance of our interface in a user study and used an off-the-shelf joystick as a comparison. Results of the study illustrated several advantages of our proposed interface. First, the trackball interface with haptic feedback resulted in the best performance in both precisely following a given path and avoiding obstacles during navigation. This result therefore illustrates the potential for improved accuracy and safety enabled with our interface. Second, the fact that the trackball interface, even without haptic feedback, still resulted in better performance than using the joystick for the above metrics, shows the potential advantage of our proposed system architecture compared to conventional joysticks.

Future work will include additional studies, as well as several improvements to the device design and control. In particular, although we expected the performance with haptic feedback to be significantly better than that without, in some cases the performance was very similar. We believe that the benefits of providing haptic feedback will become even more apparent when performing highly complex tasks. Future studies will therefore include navigation through more constrained environments, and will also investigate the learning curves for the device both with and without feedback. In addition, our system is currently designed to control just the tip position of the robot and not the entire shape. We will take two different approaches to improving this aspect of the device, including creating an algorithm for adjusting the body shape in real-time based on the task and environment, and extending the current design to include additional controllable degrees of freedom. Finally, the proposed interface has the potential to be used as a leader device for many other robots beyond the tendon-driven continuum robot shown here, and, based on these initial studies, the interface shows great promise for improving performance in such teleoperation tasks.

References

[1] G. Robinson and J. B. C. Davies, "Continuum robots- a state of the art," in *IEEE Int. Conf. on Robotics and Automation*, vol. 4, 1999, pp. 2849–2854.

[2] J. Burgner-Kahrs, D. C. Rucker, and H. Choset, "Continuum robots for medical applications: A survey," *IEEE Transactions on Robotics*, vol. 31, no. 6, pp. 1261–1280, 2015.

[3] I. D. Walker, "Continuous backbone "continuum" robot manipulators," *International Scholarly Research Notices*, vol. 2013, pp. 1–19, 2013.

[4] S. Neppalli and B. A. Jones, "Design, construction, and analysis of a continuum robot," *IEEE/RSJ Int. Conf. on Intelligent Robots and Systems*, pp. 1503–1507, 2007.

[5] C. Fellmann, D. Kashi, and J. Burgner-Kahrs, "Evaluation of input devices for teleoperation of concentric tube continuum robots for surgical tasks," in *Medical Imaging 2015: Image-Guided Procedures, Robotic Interventions, and Modeling*, vol. 9415. SPIE, 2015, pp. 411–419.

[6] M. Csencsits, B. A. Jones, W. McMahan, V. Iyengar, and I. D. Walker, "User interfaces for continuum robot arms," *IEEE/RSJ Int. Conf. on Intelligent Robots and Systems*, pp. 3123–3130, 2005.

[7] S. Omari, M.-D. Hua, G. Ducard, and T. Hamel, "Bilateral haptic teleoperation of vtol uavs," in *IEEE Int. Conf. on Robotics and Automation*, 2013, pp. 2393–2399.

[8] K. W. Ng, R. Mahony, and D. Lau, "A dual joystick-trackball interface for accurate and time-efficient teleoperation of cable-driven parallel robots within large workspaces," *Int. Conf. on Cable-Driven Parallel Robots*, vol. 74, 2019.

[9] S. Bhattacherjee, S. Chattopadhayay, V. Rao, S. Seth, S. Mukherjee, A. Sengupta, and S. Bhaumik, "Kinematics and teleoperation of tendon driven continuum robot," *Procedia Computer Science*, vol. 133, pp. 879–886, 2018.

[10] B. Ouyang, Y. Liu, H.-Y. Tam, and D. Sun, "Design of an interactive control system for a multisection continuum robot," *IEEE/ASME Transactions on Mechatronics*, vol. 23, no. 5, pp. 2379–2389, Oct 2018.

[11] Y. B.-J. Yoon H-S, "Design of a master device for controlling multi-moduled continuum robots," *Proceedings of the Institution of Mechanical Engineers, Part C: Journal of Mechanical Engineering Science*, vol. 231, no. 10, pp. 1921–1931, 2017.

[12] H. El-Hussieny, U. Mehmood, Z. Mehdi, S.-G. Jeong, M. Usman, E. W. Hawkes, A. M. Okamura, and J.-H. Ryu, "Development and evaluation of an intuitive flexible interface for teleoperating soft growing robots," *IEEE/RSJ Int. Conf. on Intelligent Robots and Systems*, pp. 4995–5002, 2018.

[13] C. G. Frazelle, A. Kapadia, and I. Walker, "Developing a kinematically similar master device for extensible continuum robot manipulators," *Journal of Mechanisms and Robotics*, vol. 10, no. 2, p. 025005, 2018.

[14] C. R. Wagner, R. D. Howe, and N. Stylopoulos, "The role of force feedback in surgery: analysis of blunt dissection," in *Int. Symposium on Haptic Interfaces for Virtual Environment and Teleoperator Systems*, 2002, pp. 73–73.

[15] J. Burgner, D. C. Rucker, H. B. Gilbert, P. J. Swaney, P. T. Russell, K. D. Weaver, and R. J. Webster, "A telerobotic system for transnasal surgery," *IEEE/ASME Transactions on Mechatronics*, vol. 19, no. 3, pp. 996–1006, 2013.

[16] A. H. Gosline, N. V. Vasilyev, E. J. Butler, C. Folk, A. Cohen, R. Chen, N. Lang, P. J. Del Nido, and P. E. Dupont, "Percutaneous intracardiac beating-heart surgery using metal mems tissue approximation tools," *The International Journal of Robotics Research*, vol. 31, no. 9, pp. 1081–1093, 2012.

[17] R. J. Webster, T. E. Murphy, L. N. Verner, and A. M. Okamura, "A novel two-dimensional tactile slip display: Design, kinematics and perceptual experiments," *ACM Trans. Appl. Percept.*, vol. 2, no. 2, p. 150–165, 2005.

[18] S. Kianzad and K. E. MacLean, "Harold's purple crayon rendered in haptics: Large-stroke, handheld ballpoint force feedback," *IEEE Haptics Symposium*, 2018.

[19] T. E. Murphy, R. Webster, and A. Okamura, "Design and performance of a two-dimensional tactile slip display," in *Eurohaptics*, 2004, pp. 130–137.

[20] M. Choi and G. J. Kim, "Touchball: a design and evaluation of a hand-held trackball based touch-haptic interface," in *Proceedings of the SIGCHI Conference on Human Factors in Computing Systems*, 2009, pp. 1535–1538.

[21] Y. Tsumaki, T. Ohgi, and A. Niiyama, "A spherical haptic interface with unlimited workspace," *International Journal on Smart Sensing and Intelligent Systems*, vol. 3, no. 3, 2017.

[22] I. Robert J. Webster and B. A. Jones, "Design and kinematic modeling of constant curvature continuum robots: A review," *The International Journal of Robotics Research*, vol. 29, no. 13, pp. 1661–1683, 2010.